EUROPEAN JOURNAL OF PURE AND APPLIED MATHEMATICS
2025, Vol. 18, Issue 2, Article Number 5892
ISSN 1307-5543 – ejpam.com
Published by New York Business Global

Qualitative Study on Finite Volume Method for Solving Linear and Nonlinear Partial Differential Equations

Thekra Abdullah Fayez Alfawaz[1], Abdulkafi Mohammed Saeed[1,*]

[1] *Department of Mathematics, College of Science, Qassim University, Buraydah, Kingdom of Saudi Arabia*

Abstract. Numerous numerical solutions have been developed over the past decades to provide suitable solutions for several types of problems in computational fluid dynamics (CFD). The finite volume method (FVM) is a numerical technique adopted in computational fluid dynamics to solve partial differential equations representing conservation laws. In this article, two mathematical models are presented: one for the linear advection equation and another for the nonlinear Burgers' equation with diffusion, along with various schemes of the FVM. Furthermore, numerical experiments will be conducted for several FVM schemes to demonstrate the most effective approach for solving the studied problem.

2020 Mathematics Subject Classifications: 76S05, 76D10, 80A32, 35Q79

Key Words and Phrases: Linear advection equation, nonlinear Burgers' equation, finite volume method, computational fluid dynamics, error analysis

1. Introduction

Computational fluid dynamics (CFD) is the analysis of systems involving fluid flow, heat transfer, and associated phenomena such as chemical reactions using computer-based simulation. This powerful technique is applied across a broad spectrum of both industrial and non-industrial fields [1].

The finite volume method (FVM) is a numerical approach that converts partial differential equations, which describe conservation laws over infinitesimal volumes, into discrete algebraic equations for finite volumes. It has evolved to address complex situations in computational fluid dynamics and has been adapted to study intricate physical phenomena, including magneto-elastic semiconductor interactions [2], wave interactions in functionally graded materials [3], and solitary wave solutions in plasma physics [4].

The FVM process includes a range of computational complexities, from mesh generation to the application of boundary conditions [1].

*Corresponding author.
DOI: https://doi.org/10.29020/nybg.ejpam.v18i2.5892

Email addresses: 441212381@qu.edu.sa (T. ALfawaz), abdulkafi.ahmed@qu.edu.sa (A.M. Saeed)

The finite volume method has been used by researchers to solve numerous problems related to computational fluid dynamics, as in the development of an arbitrary Lagrangian-Eulerian formulation for compressible flows based on the multi-moment finite volume method [5]. In addition, FVM is used to describe the Navier-Stokes equations and their solutions [6, 7] and in incompressible flow problems which cover a wide range of physical phenomena such as environmental and geophysical flows and the dynamics of mechanical processes [8, 9].

In the FVM, different schemes exhibit unique characteristics, such as conservativeness, boundedness, and transportiveness. Examples of these schemes include upwind differencing scheme, central differencing scheme, essentially nonoscillatory (ENO) scheme, and other related schemes [10, 11].

The main purpose of this paper is to investigate the most efficient schemes in the finite volume method to solve a one-dimensional linear advection equation and a two-dimensional nonlinear Burgers' equation with diffusion. The FVM will be formulated and applied to solve these problems, and numerical experiments will be performed to compare the approximate solutions with the exact ones.

The following is the outline of this paper: In Section 2, the central differencing scheme is introduced, followed by Section 3, which covers the upwind differencing scheme. Section 4 presents a brief description of the Essentially Non-Oscillatory (ENO) scheme, and Section 5 details the Weighted Essentially Non-Oscillatory (WENO) scheme. Section 6 presents numerical experiments to assess the performance of these schemes. Section 7 discusses the results. Finally, Section 8 concludes the paper and suggests directions for future research, particularly focusing on extending another scheme.

2. Central differencing scheme

In this scheme, the computational domain is discretized into a finite number of control volumes. The main concept is to approximate the fluxes at the boundaries of each control volume using central differences, which provide second-order accuracy. In particular, the value of the variable at the cell faces is calculated as the average of the values at the neighboring cell centers. Mathematically, this is expressed as:

$$f_{i+\frac{1}{2}} = \frac{f_i + f_{i+1}}{2}, \tag{1}$$

where
$f_{i+\frac{1}{2}}$ represents the value at the interface between cells i and $i+1$.
f_i and f_{i+1} represent the values at the centers of cells i and $i+1$, respectively [1].

3. Upwind differencing scheme

This scheme relies on the principle of causality, utilizing information from the direction of the flow to compute fluxes at the control volume boundaries. Particularly, the value at

the cell face is determined using the value from the upstream cell, which helps to maintain stability and reduce numerical oscillations. Mathematically, this is represented as:

$$f_{i+\frac{1}{2}} = \begin{cases} f_i & \text{if } u > 0, \\ f_{i+1} & \text{if } u < 0, \end{cases} \tag{2}$$

where
$f_{i+\frac{1}{2}}$ denotes the flux at the interface between control volumes i and $i+1$.
u is the velocity of the flow.
f_i represents the values at the center of cell i [1].

4. Essentially Non-Oscillatory (ENO) scheme

Essentially Non-Oscillatory (ENO) schemes started with the classic paper of Harten, Engquist, Osher, and Chakravarthy [12]. The ENO schemes are high-order accurate and effectively capture shocks with sharp, visually monotonic transitions. The schemes of ENO are well-suited for problems containing both shocks and complicated smooth flow structures.

Additionally, ENO schemes depending on point values and TVD Runge-Kutta time discretization, which can reduce computational costs significantly for multi-space dimensions, although ENO schemes choose the smoothest stencil to capture discontinuities from a set of candidate approximation stencils [13, 14].

5. Weighted Essentially Non-Oscillatory (WENO) scheme

The key advantage of Weighted Essentially Non-Oscillatory (WENO) schemes is their ability to present high accuracy while avoiding spurious oscillations near discontinuities, such as shocks or contact discontinuities. Furthermore, WENO schemes are capable of achieving high-order accuracy (third, fifth, or even higher) in smooth regions, making them highly attractive for problems requiring high precision. These features make WENO schemes ideal for simulating fluid dynamics, wave propagation, and other problems involving discontinuities.

WENO schemes have gained more attention than Essentially Non-Oscillatory (ENO) schemes, both in algorithm development and applications. Unlike ENO, which is based on a single interpolation or reconstruction using one selected stencil, WENO employs a convex combination of interpolations from multiple candidate stencils. The weights in WENO schemes are specifically designed to retain the ENO property for capturing discontinuities while restoring the background linear scheme in smooth regions of the solution. This dual feature ensures accuracy and stability, making WENO schemes particularly effective for addressing the discontinuities present in many complex problems [13–15].

In the paper, two classifications of the method will be discussed:

(i) The 3^{rd} -order Weighted Essentially Non-Oscillatory (WENO3).

(ii) The 5^{th} -order Weighted Essentially Non-Oscillatory (WENO5).

5.1. WENO methodology in FVM framework

A general system of hyperbolic conservation laws:

$$\frac{\partial u}{\partial t} + \sum_{i=1}^{d} \frac{\partial}{\partial x_i} f_i(u) = 0, \tag{3}$$

is considered where d is the space dimension, u is the solution vector, and $f_i(u)$ is the physical flux in the i-th direction.

The computational domain in space is defined as $\Omega = \left[x^L, x^R\right]$, which is divided into N cells represented by I_i such as $I_i = \left[x_{i-\frac{1}{2}}, x_{i+\frac{1}{2}}\right]$. Following that, the grid size within the domain is given by $\Delta x_i = x_{i+\frac{1}{2}} - x_{i-\frac{1}{2}}$, and the cell centers are located at $x_i = \frac{1}{2}\left(x_{i-\frac{1}{2}} + x_{i+\frac{1}{2}}\right)$ where $i = 1, 2, \ldots, N$.

For simplicity, considering the one-dimensional scalar hyperbolic conservation law:

$$\frac{\partial u}{\partial t} + \frac{\partial}{\partial x} f(u) = 0, \tag{4}$$

with the initial condition: $u(x, 0) = u_0(x)$

Applying the finite volume method to Equation (4) and integrating over the cell $I_i = \left[x_{i-\frac{1}{2}}, x_{i+\frac{1}{2}}\right]$, the conservation law becomes:

$$\frac{d}{dt} \int_{x_{i-\frac{1}{2}}}^{x_{i+\frac{1}{2}}} u(x,t)dx + \left[f(u(x,t))|_{x_{i+\frac{1}{2}}} - f(u(x,t))|_{x_{i-\frac{1}{2}}} \right] = 0, \tag{5}$$

Where $f(u)$ is the physical flux, which may be approximated by its numerical counterpart $\hat{f}$ (referred to as the numerical flux), and $\bar{u}_i(t)$ be the average value of the solution $u(x, t)$ over the cell I_i for all i :

$$\bar{u}_i(t) = \frac{1}{\Delta x} \int_{x_{i-\frac{1}{2}}}^{x_{i+\frac{1}{2}}} u(x,t)dx, \tag{6}$$

where Δx is the width of the cell.

Substituting this cell-averaged value into the finite volume formulation, the semi-discrete form of the conservation law becomes:

$$\frac{d}{dt}\bar{u}_i(t) = -\frac{1}{\Delta x}\left[f\left(u\left(x_{i+\frac{1}{2}}, t\right)\right) - f\left(u\left(x_{i-\frac{1}{2}}, t\right)\right)\right], \tag{7}$$

Where $\Delta x = x_{i+\frac{1}{2}} - x_{i-\frac{1}{2}}$ approximating Equation (7) using the following conservative scheme, yields a system of ordinary differential equations (ODEs), leading to the semi-discrete finite volume scheme:

$$\frac{d}{dt}\bar{u}_i(t) = -\frac{1}{\Delta x}\left(\hat{f}_{i+\frac{1}{2}} - \hat{f}_{i-\frac{1}{2}}\right), \tag{8}$$

The numerical flux $\hat{f}_{i\pm1/2}$ is given by the following expression:

$$\hat{f}_{i\pm1/2} = h\left(u^{-}_{i\pm\frac{1}{2}}, u^{+}_{i\pm\frac{1}{2}}\right), \tag{9}$$

to obtain the semi-discrete finite volume scheme

$$\frac{d}{dt}\bar{u}_i(t) + \frac{1}{\Delta x}\left[h\left(u^{-}_{i+\frac{1}{2}}, u^{+}_{i+\frac{1}{2}}\right) - h\left(u^{-}_{i-\frac{1}{2}}, u^{+}_{i-\frac{1}{2}}\right)\right] = 0, \tag{10}$$

When the values $u^{\pm}_{i+\frac{1}{2}}$ and $u^{\pm}_{i-\frac{1}{2}}$ were reconstructed by WENO method and using the Runge-Kutta method to solve the resulting of ODEs in (8).

The function $h(a, b)$ in expression (9) is a monotone numerical flux that meets specific conditions, there are some examples of monotone fluxes include the Godunov flux, Engquist-Osher flux, and Lax-Friedrichs flux [13, 16].

The goal of WENO reconstruction is to compute the interface values $u^{\pm}_{i+\frac{1}{2}}$ and $u^{\pm}_{i-\frac{1}{2}}$ by forming a convex combination of all candidate reconstructions $u^{(r)}_{i\pm\frac{1}{2}}$. This involves combining k candidate stencils S_r, each stencil provides sets of neighboring cell values

$$S_r(i) = \{x_{i-r}, x_{i-r+1}, \ldots, x_{i-r+k-1}\}, \quad r = 0, \ldots, k-1. \tag{11}$$

For each stencil, generate k different reconstructions for the solution values at the cell boundaries $x_{i\pm\frac{1}{2}}$, These reconstructions are computed as:

$$u^{(r)}_{i+\frac{1}{2}} = \sum_{j=0}^{k-1} C_{rj}\bar{u}_{i-r+j}, \quad u^{(r)}_{i-\frac{1}{2}} = \sum_{j=0}^{k-1} \tilde{C}_{rj}\bar{u}_{i-r+j}, \tag{12}$$

where C_{rj} and $\tilde{C}_{rj}$ are the reconstructed value at the cell boundary $x_{i+\frac{1}{2}}$ and $x_{i-\frac{1}{2}}$ respectively.

The key to the success of WENO would be the choice of the weights ω_r, each stencil is assigned a nonlinear weight ω_r, which is computed based on the smoothness indicators as follows:

$$\omega_r = \frac{\alpha_r}{\sum_{s=0}^{k-1}\alpha_s}, \quad \widetilde{\omega}_r = \frac{\tilde{\alpha}_r}{\sum_{s=0}^{k-1}\tilde{\alpha}_s}, \tag{13}$$

with

$$\alpha_r = \frac{d_r}{(\varepsilon+\beta_r)^2}, \quad \tilde{\alpha}_r = \frac{\tilde{d}_r}{(\varepsilon+\beta_r)^2}, \quad r = 0, \ldots, k-1. \tag{14}$$

where the nonlinear weights satisfy: $\omega_r \geq 0$, $\sum_{r=0}^{k-1}\omega_r = 1$, and ε is a small number which must satisfy: $\varepsilon \geq 0$.

Each stencil is assigned a smoothness indicator β_r that is used to measure the smoothness of stencil polynomials, it is used in the calculation of weights, and it constructs weights such that the discontinuity is avoided inside the stencil, and it's given as following:

$$\beta_r = \sum_{l=1}^{k-1}\int_{x_{i-\frac{1}{2}}}^{x_{i+\frac{1}{2}}} \Delta x^{2l-1}\left(\frac{\partial^l p_r(x)}{\partial x^l}\right)^2 dx, \quad \forall r = 0, \ldots, k-1. \tag{15}$$

The right-hand side of Equation (15) represents the sum of the squares of scaled L^2 norms for all the derivatives of the interpolation polynomial $p_r(x)$ evaluated over the specified interval I_i on the stencil $S_r(i)$. The factor Δx^{2l-1} is introduced to remove any Δx dependency in the derivatives.

If the function $u(x)$ is smooth in all the candidate stencils there are constants d_r such that

$$u_{i+\frac{1}{2}} = \sum_{r=0}^{k-1} d_r u_{i+\frac{1}{2}}^{(r)} = u\left(x_{i+\frac{1}{2}}\right) + O\left(\Delta x^{2k-1}\right), \tag{16}$$

$$u_{i-\frac{1}{2}} = \sum_{r=0}^{k-1} \tilde{d}_r u_{i-\frac{1}{2}}^{(r)} = u\left(x_{i-\frac{1}{2}}\right) + O\left(\Delta x^{2k-1}\right), \tag{17}$$

where d_r is always positive and $\sum_{r=0}^{k-1} d_r = 1$, and by symmetry $\tilde{d}_r = d_{k-1-r}$. In this smooth case, to keep the order of accuracy $(2k-1)$, then ω_r should be

$$\omega_r = d_r + O\left(\Delta x^{k-1}\right), \quad r = 0, \ldots, k-1. \tag{18}$$

which would imply order of accuracy $(2k-1)^{\text{th}}$ order of accuracy

$$u_{i+\frac{1}{2}}^{-} = \sum_{r=0}^{k-1} \omega_r u_{i+\frac{1}{2}}^{(r)} = u\left(x_{i+\frac{1}{2}}\right) + O\left(\Delta x^{2k-1}\right), \tag{19}$$

$$u_{i-\frac{1}{2}}^{+} = \sum_{r=0}^{k-1} \widetilde{\omega}_r u_{i-\frac{1}{2}}^{(r)} = u\left(x_{i-\frac{1}{2}}\right) + O\left(\Delta x^{2k-1}\right), \tag{20}$$

here, ω_r and $\widetilde{\omega}_r$, defined in (13), are constructed based on the smoothness indicators [13, 15–18].

5.2. Time discretization for WENO scheme

After the spatial derivative is discretized with the WENO scheme, a set of ordinary differential equations (ODEs) is obtained as:

$$\frac{du}{dt} = L(u), \tag{21}$$

where L denotes the spatial discretization operator represented in (8). The general m-stage Runge-Kutta (RK) method is written as:

$$\begin{gathered} u^{(i)} = \sum_{k=0}^{i-1} \left(\alpha_{ik} u^{(k)} + \Delta t \beta_{ik} L\left(u^{(k)}\right)\right), \quad i = 1, \ldots, m. \\ u^{(0)} = u^{(n)}, \quad u^{(m)} = u^{(n+1)}, \end{gathered} \tag{22}$$

The set of ODEs in this paper can be discretized by a 3^{rd} -order by total variation diminishing (TVD) Runge-Kutta method as follows [13, 19]:

$$\begin{aligned} u^{(1)} &= u^{(n)} + \Delta t L\left(u^{(n)}\right), \\ u^{(2)} &= \frac{3}{4}u^{(n)} + \frac{1}{4}u^{(1)} + \frac{1}{4}\Delta t L\left(u^{(1)}\right), \\ u^{(n+1)} &= \frac{1}{3}u^{(n)} + \frac{2}{3}u^{(2)} + \frac{2}{3}\Delta t L\left(u^{(2)}\right). \end{aligned} \tag{23}$$

6. Numerical experiments

In this section, two numerical experiments will be carried out to solve linear advection of multiple waves and two-dimensional Burgers' equation with diffusion for comparison purposes and to verify the results.

6.1. Linear advection of multiple waves

Considering the one-dimensional linear advection equation:

$$\frac{\partial \mathrm{u}}{\partial \mathrm{t}} + \frac{\partial \mathrm{u}}{\partial \mathrm{x}} = 0, \tag{24}$$

With the initial condition:

$$u(x,0) = \begin{cases} \frac{1}{6}[G(x-1,\beta,z-\theta) + G(x-1,\beta,z+\theta) + 4G(x-1,\beta,z)], & \text{if } 0.2 \le x < 0.4, \\ 1, & \text{if } 0.6 \le x \le 0.8, \\ 1 - |10(x-1.1)|, & \text{if } 1.0 \le x \le 1.2, \\ \frac{1}{6}[F(x-1,\alpha,a-\theta) + F(x-1,\alpha,a+\theta) + 4F(x-1,\alpha,a)], & \text{if } 1.4 \le x < 1.6, \\ 0, & \text{otherwise,} \end{cases} \tag{25}$$

where:

$$G(x,\beta,z) = e^{-\beta(x-z)^2}, \quad F(x,\alpha,a) = \sqrt{\max\left(1-\alpha^2(x-a)^2, 0\right)}. \tag{26}$$

with parameters:

$$a = 0.5, \quad z = -0.7, \quad \theta = 0.005, \quad \alpha = 10, \quad \beta = \frac{\log(2)}{36\theta^2}. \tag{27}$$

The initial condition consists of a Gaussian pulse, a square wave, a sharp triangle wave, and a half ellipse arranged from the left to the right in the computational domain $x \in [0, 2]$. The exact solution, representing the theoretical solution for the linear advection equation with a constant propagation speed c, is:

$$u(x,t) = u_0(x - ct). \tag{28}$$

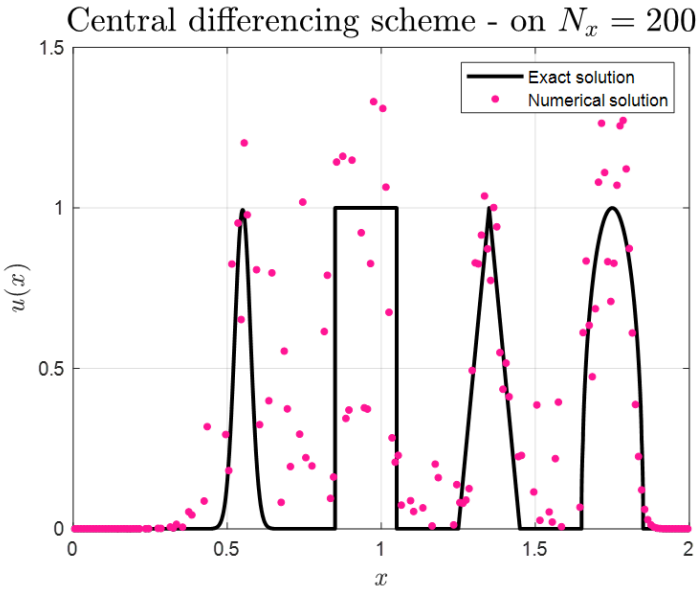

Figure 1: One-dimensional linear advection of multiple waves in showing the exact solution vs. the numerical solution, along with the u distributions obtained from the central differencing scheme at simulation time $t = 0.5$. The spatial discretization is performed on 200 uniform grid points with a Courant number of $CFL = 0.5$.

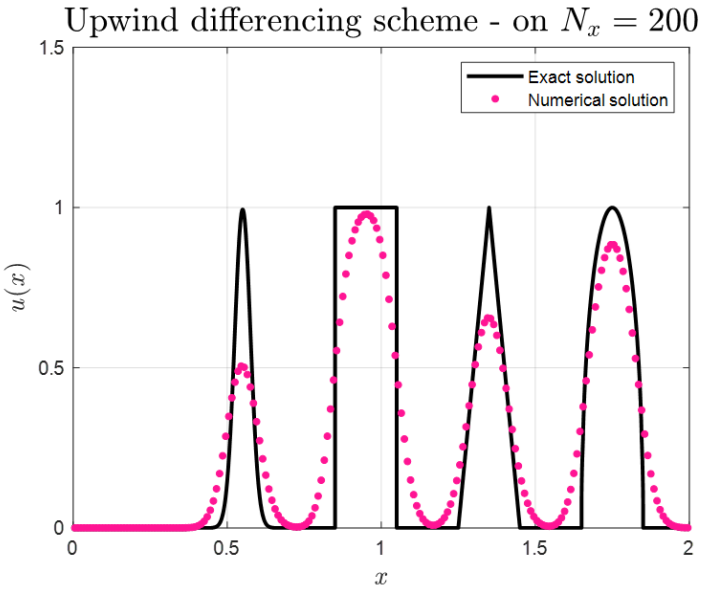

Figure 2: One-dimensional linear advection of multiple waves in showing the exact solution vs. the numerical solution, along with the u distributions obtained from the upwind differencing scheme at simulation time $t = 0.5$. The spatial discretization is performed on 200 uniform grid points with a Courant number of $CFL = 0.5$.

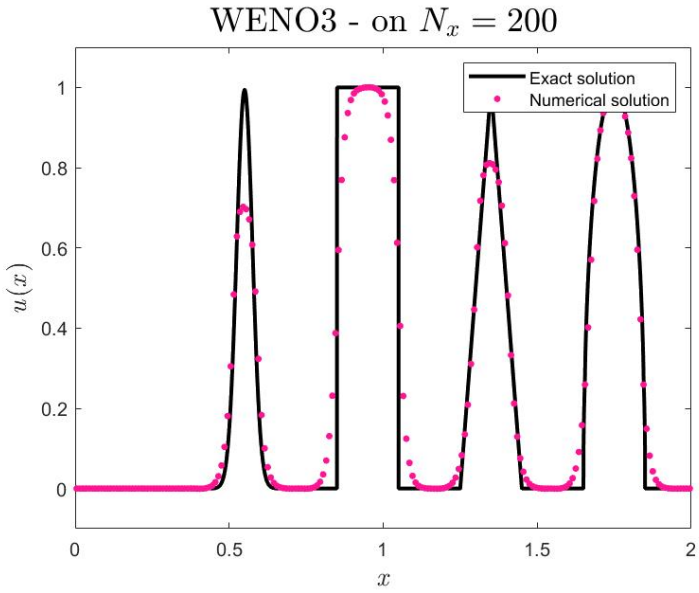

Figure 3: One-dimensional linear advection of multiple waves in showing the exact solution vs. the numerical solution, along with the u distributions obtained from the WENO3 scheme at simulation time $t = 0.5$. The spatial discretization is performed on 200 uniform grid points with a Courant number of $CFL = 0.5$.

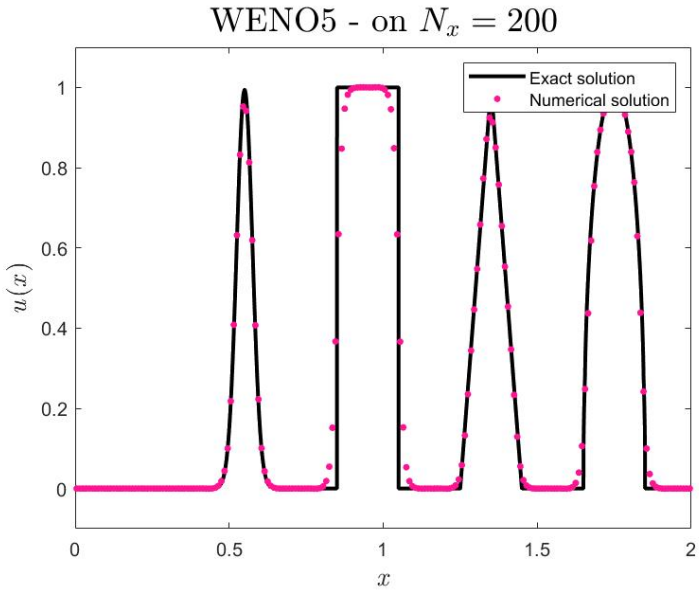

Figure 4: One-dimensional linear advection of multiple waves in showing the exact solution vs. the numerical solution, along with the u distributions obtained from the WENO5 scheme at simulation time $t = 0.5$. The spatial discretization is performed on 200 uniform grid points with a Courant number of $CFL = 0.5$.

Table 1: Error analysis for central differencing scheme in FVM framework at $CFL = 0.5$.

N_x \ scheme		Central differencing scheme
25	L_1 **error**	0.65607
	L_2 **error**	0.59542
	L_∞ **error**	0.94175
50	L_1 **error**	0.48812
	L_2 **error**	0.44254
	L_∞ **error**	0.68826
100	L_1 **error**	0.4083
	L_2 **error**	0.39903
	L_∞ **error**	0.93897
200	L_1 **error**	0.39833
	L_2 **error**	0.43939
	L_∞ **error**	1.1754

Table 2: Error analysis for upwind differencing scheme in FVM framework at $CFL = 0.5$.

N_x \ scheme		Upwind differencing scheme
25	L_1 **error**	0.50568
	L_2 **error**	0.4245
	L_∞ **error**	0.60352
50	L_1 **error**	0.37711
	L_2 **error**	0.33849
	L_∞ **error**	0.63623
100	L_1 **error**	0.27896
	L_2 **error**	0.27365
	L_∞ **error**	0.61025
200	L_1 **error**	0.18559
	L_2 **error**	0.20518
	L_∞ **error**	0.47363

Table 3: Error analysis for WENO3 and WENO5 in FVM framework at $CFL = 0.5$.

N_x \ scheme		WENO3	WENO5
25	L_1 **error**	0.47798	0.34751
	L_2 **error**	0.41071	0.32829
	L_∞ **error**	0.68641	0.6715
50	L_1 **error**	0.27409	0.18028
	L_2 **error**	0.26617	0.20625
	L_∞ **error**	0.58412	0.45793
100	L_1 **error**	0.15712	0.089675
	L_2 **error**	0.18883	0.13884
	L_∞ **error**	0.51135	0.50284
200	L_1 **error**	0.077098	0.035365
	L_2 **error**	0.11764	0.083419
	L_∞ **error**	0.40532	0.36654

6.2. Burgers' equation with diffusion

Considering the two-dimensional Burgers' equation with diffusion:

$$u_t + a\left[\left(\frac{u^2}{2}\right)_x + \left(\frac{u^2}{2}\right)_y\right] - D\left(u_{xx} + u_{yy}\right) = 0, \tag{29}$$

on the domain $[0, 2]^2$.
when $a = 1$, the exact solution is provided in Equation (30), and Figure 5 represents this solution at $CFL = 0.5$ and the final time $t = 0.5$.

$$u(x, y, t) = -2D\pi \frac{\cos(\pi(x + y)) \exp\left(-2D\pi^2 t\right)}{2 + \sin(\pi(x + y)) \exp\left(-2D\pi^2 t\right)}. \tag{30}$$

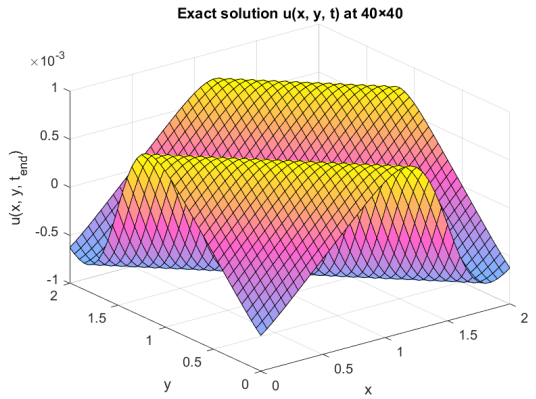

Figure 5: Exact solution of the two-dimensional Burgers' equation.

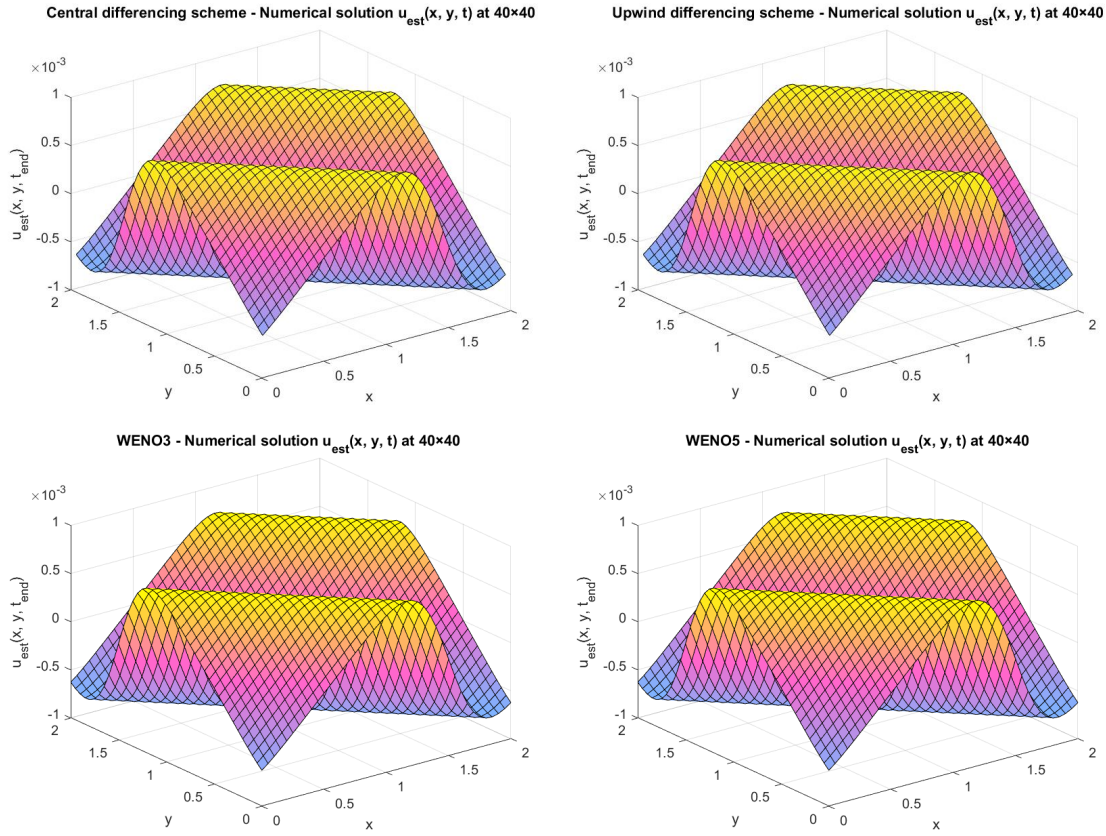

Figure 6: Two-dimensional Burgers' equation with diffusion, displaying the numerical solutions from various schemes for a diffusion coefficient $D = 0.0002$ at $CFL = 0.5$. The spatial discretization of the estimated solution $u_{est}(x, y, t)$ is performed on a 40×40 uniform grid. The numerical solutions are shown for the central differencing scheme (top left), upwind differencing scheme (top right), WENO3 (bottom left), and WENO5 (bottom right).

Table 4: Error analysis for central differencing scheme in FVM framework for a diffusion coefficient $D = 0.0002$ at $CFL = 0.5$.

$N_x \times N_y$ \ scheme		Central differencing scheme
20×20	L_1 error	8.2763e-07
	L_2 error	1.093e-06
	L_∞ error	2.051e-06
40×40	L_1 error	4.2254e-07
	L_2 error	7.8345e-07
	L_∞ error	2.0943e-06
80×80	L_1 error	2.1277e-07
	L_2 error	5.575e-07
	L_∞ error	2.0943e-06
160×160	L_1 error	1.1087e-07
	L_2 error	3.9544e-07
	L_∞ error	2.0977e-06

Table 5: Error analysis for the upwind differencing scheme in FVM framework for a diffusion coefficient $D = 0.0002$ at $CFL = 0.5$.

$N_x \times N_y$ \ scheme		Upwind differencing scheme
20×20	L_1 error	1.3824e-06
	L_2 error	1.1794e-06
	L_∞ error	2.051e-06
40×40	L_1 error	7.5091e-07
	L_2 error	8.2257e-07
	L_∞ error	2.0943e-06
80×80	L_1 error	3.9118e-07
	L_2 error	5.7267e-07
	L_∞ error	2.0943e-06
160×160	L_1 error	1.9917e-07
	L_2 error	4.0102e-07
	L_∞ error	2.0977e-06

Table 6: Error analysis for WENO3 and WENO5 in FVM framework for a diffusion coefficient $D = 0.0002$ at $CFL = 0.5$.

$N_x \times N_y$ \ scheme		WENO3	WENO5
20×20	L_1 error	1.6834e-07	5.126e-08
	L_2 error	2.0541 e-07	6.5106e-08
	L_∞ error	3.3108e − 07	1.3088 -07
40×40	L_1 error	2.2e − 07	5.3135e-08
	L_2 error	2.5939e-07	6.1183e-08
	L_∞ error	4.7755e − 07	9.6984e − 08
80×80	L_1 error	2.3917 - 07	7.1989e-08
	L_2 error	2.8305e-07	8.4092e-08
	L_∞ error	5.6877e-07	1.6397e-07
160×160	L_1 error	2.4296 e-07	7.4868e-08
	L_2 error	2.8789e-07	8.8955e-08
	L_∞ error	5.9143e − 07	1.884e − 07

7. Discussion

The linear advection of multiple waves equation displays the effectiveness of different numerical schemes in capturing the dynamics of multiple waveforms. In the first case, the initial condition provides a comprehensive test to assess the accuracy of the numerical methods employed.

Simulations confirm that the central differential scheme despite its simplicity and computational ease results in relatively high error levels particularly for the L_2 and L_∞ norms as presented in Table 1. It is essential to highlight that errors are significantly reduced when employing the upwind differencing scheme which demonstrates greater stability for advection-dominated problems as shown in Table 2. This strategy, even so, is still less accurate compared to the Weighted Essentially Non-Oscillatory (WENO) scheme.

The WENO3 and WENO5 schemes as presented in Table 3 show considerably lower errors across all norms with WENO5 particularly excelling in its ability to resolve steep gradients and discontinuities more effectively than lower-order methods. Visual comparisons in Figure 1, 2, 3 and 4 support these findings.

Figure 7 presents a combined plot that compares the performance of all the schemes, highlighting the strengths and weaknesses of each scheme.

They confirm that WENO methods maintain the integrity of the wave shapes over time while the central differencing scheme and upwind differencing scheme patterns reveal significant diffusion and distortion of the wave profiles.

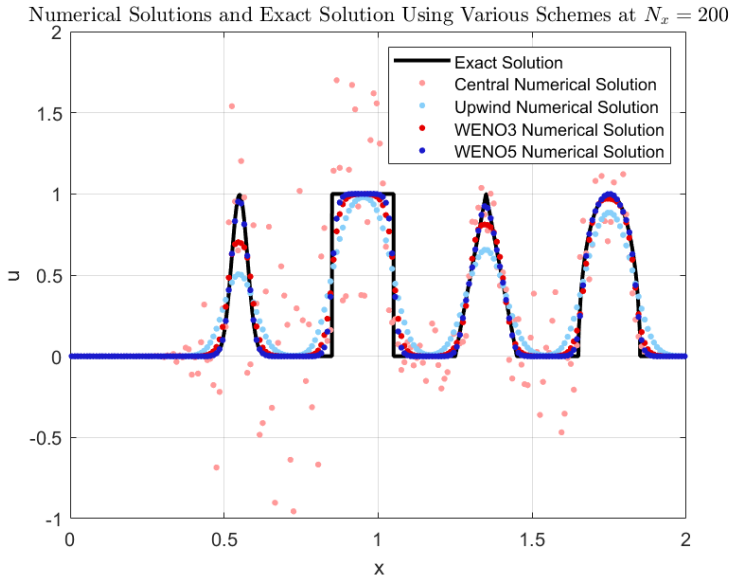

Figure 7: Linear advection of multiple waves using various schemes at simulation time $t = 0.5$. The spatial discretization is performed on 200 uniform grid points with a Courant number of $CFL = 0.5$.

The two-dimensional Burgers' equation with diffusion and the numerical solutions received from different schemes provide insights into the interplay between advection and diffusion.
The exact solution for the diffusion coefficient $D = 0.0002$ as presented in Figure 5 provides a benchmark for estimating the performance of numerical methods.
The error analysis presented in Tables 4 and 5 implies that the central differencing scheme achieves an acceptable level of accuracy but the errors remain substantial, particularly in the L_∞ norm while the upwind differencing scheme improves upon this improvement but remains incapable of capturing the finer details of the solution.
The WENO3 and WENO5 schemes in Table 6, continue to excel the lower-order methods and achieve substantially lower error values.
This is particularly apparent in their ability to resolve the solution's features as represented in Figure 6. The high fidelity of the WENO schemes especially is essential for applications involving sharp gradients where diffusion plays a critical role in the solution behavior.

8. Conclusion

This study rigorously examines numerical solutions to the one-dimensional linear advection equation and the two-dimensional Burgers' equation using the Weighted Essentially Non-Oscillatory (WENO5) method. The results demonstrate significantly lower error rates across various norms, including $L_1, L_2,$ and L_∞. The superior performance of WENO5 is particularly evident when compared to lower-order schemes.
Specifically, this research establishes that WENO5 outperforms other methods, such as

WENO3, central differencing, and upwind differencing, particularly in scenarios characterized by sharp gradients. This capability highlights WENO5's proficiency in addressing complex fluid dynamics problems where accuracy is paramount.

Future research may focus on extending other advanced numerical schemes, such as the Targeted Essentially Non-Oscillatory (TENO) scheme. Investigating its methodological techniques could lead to further improvements in computational efficiency and accuracy, potentially broadening its applicability to a diverse range of fluid dynamics challenges.

Acknowledgements

The Researchers would like to thank the Deanship of Graduate Studies and Scientific Research at Qassim University for financial support (QU-APC-2025). They also extend their appreciation to the anonymous reviewers for their insightful suggestions, which have greatly improved the quality of the manuscript.

References

[1] Fadl Moukalled, Luca Mangani, Marwan Darwish, F Moukalled, L Mangani, and M Darwish. *The finite volume method*. Springer, 2016.

[2] Kh Lotfy, AA El-Bary, W Hassan, and MH Ahmed. Hall current influence of microtemperature magneto-elastic semiconductor material. *Superlattices and Microstructures*, 139:106428, 2020.

[3] Kh Lotfy and RS Tantawi. Photo-thermal-elastic interaction in a functionally graded material (fgm) and magnetic field. *Silicon*, 12(2):295–303, 2020.

[4] Abdulghani R Alharbi, MB Almatrafi, and Kh Lotfy. Constructions of solitary travelling wave solutions for ito integro-differential equation arising in plasma physics. *Results in Physics*, 19:103533, 2020.

[5] Peng Jin, Xi Deng, and Feng Xiao. An ale formulation for compressible flows based on multi-moment finite volume method. *Engineering Applications of Computational Fluid Mechanics*, 12(1):791–809, 2018.

[6] Stelian Ion and Anca Veronica Ion. A finite volume method for solving generalized navier-stokes equations. *Annals of the Academy of Romanian Scientists: Series on Mathematics and its Applications*, 3:145–163, 2011.

[7] David Trebotich and Daniel Graves. An adaptive finite volume method for the incompressible navier–stokes equations in complex geometries. *Communications in Applied Mathematics and Computational Science*, 10(1):43–82, 2015.

[8] Walter Boscheri, Andrea Chiozzi, Michele Giuliano Carlino, and Giulia Bertaglia. A new family of semi-implicit finite volume/virtual element methods for incompressible flows on unstructured meshes. *Computer Methods in Applied Mechanics and Engineering*, 414:116140, 2023.

[9] Dartzi Pan. A high-order finite volume method solving viscous incompressible flows using general pressure equation. *Numerical Heat Transfer, Part B: Fundamentals*, 82(5):146–163, 2022.

[10] Rainer Ansorge and Thomas Sonar. *Mathematical models of fluid dynamics: Modelling, theory, basic numerical facts-An introduction*. John Wiley & Sons, 2009.

[11] Bram van Leer and Kenneth G Powell. Introduction to computational fluid dynamics. *Encyclopedia of Aerospace Engineering*, 5:12–16, 2010.

[12] Ami Harten, Bjorn Engquist, Stanley Osher, and Sukumar R Chakravarthy. Uniformly high order accurate essentially non-oscillatory schemes, iii. *Journal of computational physics*, 131(1):3–47, 1997.

[13] Chi-Wang Shu. Essentially non-oscillatory and weighted essentially non-oscillatory schemes. *Acta Numerica*, 29:701–762, 2020.

[14] Shuhai Zhang, Jun Zhu, and Chi-Wang Shu. A brief review on the convergence to steady state solutions of euler equations with high-order weno schemes. *Advances in Aerodynamics*, 1:1–25, 2019.

[15] Pawel Buchmüller. *High-Order WENO Finite Volume Methods on Cartesian Grids with Adaptive Mesh Refinement*. PhD thesis, Dissertation, Düsseldorf, Heinrich-Heine-Universität, 2016, 2016.

[16] Y-T Zhang and C-W Shu. Eno and weno schemes. In *Handbook of numerical analysis*, volume 17, pages 103–122. Elsevier, 2016.

[17] Mohammad Afzal Shadab, Dinshaw Balsara, Wei Shyy, and Kun Xu. Fifth order finite volume weno in general orthogonally-curvilinear coordinates. *Computers & Fluids*, 190:398–424, 2019.

[18] Shantanu Shahane, Sheide Chammas, Deniz A Bezgin, Aaron B Buhendwa, Steffen J Schmidt, Nikolaus A Adams, Spencer H Bryngelson, Yi-Fan Chen, Qing Wang, Fei Sha, et al. Rational-weno: A lightweight, physically-consistent three-point weighted essentially non-oscillatory scheme. *arXiv preprint arXiv:2409.09217*, 2024.

[19] Fei Teng, Li Yuan, and Tao Tang. A speed-up strategy for finite volume weno schemes for hyperbolic conservation laws. *Journal of Scientific Computing*, 46:359–378, 2011.